

## Cryo-X-ray tomography of vaccinia virus membranes and inner compartments

José L. Carrascosa<sup>a,\*</sup>, Francisco Javier Chichón<sup>a</sup>, Eva Pereiro<sup>b</sup>, María Josefa Rodríguez<sup>a</sup>,  
Jose Jesús Fernández<sup>a,c</sup>, Mariano Esteban<sup>a</sup>, Stefan Heim<sup>d</sup>, Peter Guttmann<sup>d</sup>, Gerd Schneider<sup>d</sup>

<sup>a</sup> Centro Nacional de Biotecnología, Consejo Superior de Investigaciones Científicas (CSIC), Campus Universidad Autónoma, Madrid 28049, Spain

<sup>b</sup> ALBA Synchrotron Light Source, 08193 Bellaterra, Barcelona, Spain

<sup>c</sup> Department of Computer Architecture and Electronics, University of Almeria, 04120 Almeria, Spain

<sup>d</sup> Helmholtz-Zentrum Berlin für Materialien und Energie GmbH, Elektronenspeicherring BESSY II, Albert-Einstein-Str. 15, 12489 Berlin, Germany

### ARTICLE INFO

#### Article history:

Received 4 December 2008

Received in revised form 6 July 2009

Accepted 10 July 2009

Available online 16 July 2009

#### Keywords:

Vaccinia virus

Virion structure

Membranes

X-ray microscopy

Cryo-tomography

Electron microscopy

Three-dimensional tomographic reconstruction

### ABSTRACT

Vitrified unstained purified vaccinia virus particles have been used as a test sample to evaluate the capabilities of cryo-X-ray tomography. Embedded in a thick layer of vitreous ice, the viral particles representing the mature form of the virus (MV) were visualized using full-field transmission X-ray tomography. The tomographic reconstructions reveal the viral brick-shaped characteristic structures with a size of  $250 \times 270 \times 360 \text{ nm}^3$ . The X-ray tomograms show the presence of a clearly defined external envelope, together with an inner core surrounded by an internal envelope, including areas with clear differential density, which correlate well with those features previously described for these viral particles using electron microscopy analyses. A quantitative assessment of the resolution attained in X-ray and electron tomograms of the viral particles prepared under the same conditions yields values of 25.7 and 6.7 nm half-pitch, respectively. Although the resolution of the X-ray microscope is well above the dimensions of the membranous compartments, the strong differential contrast exhibited makes it possible to precisely reveal them without any contrasting reagent within this small and complex biological sample.

© 2009 Elsevier Inc. All rights reserved.

### 1. Introduction

The analysis of the cell at a molecular detail level to render a cartographic description of its structural components is a key aspect in the present efforts to correlate the genomic and proteomic studies into a functional system analysis at the cellular level. Cryo-electron tomography (cryo-ET) has proven to be a suitable tool in this context by combining improved preservation methods to maintain the structure and chemical composition of the samples, together with the tomographic combination of electron microscope images to allow three-dimensional reconstruction at resolutions on the order of a few nanometers (Frank, 2006; Fung et al., 1996; Grunewald and Cyrklaff, 2006; Subramaniam et al., 2007).

One of the main limitations of cryo-ET is derived from the poor penetration due to multiple scattering of electrons in soft materials (Frank, 2006; Lucic et al., 2005; Spence, 2003). Even with high voltage 300 kV microscopes equipped with energy filters, electron tomographic reconstruction is limited to about 0.5  $\mu\text{m}$  thick

samples, thus preventing the direct analysis of most cell types. Alternatively, thicker samples may be frozen to be sectioned at cryogenic temperatures, but this approach is currently limited to provide sections of 50–200 nm thickness (Dubochet et al., 1994; Frank, 2006; Tokuyasu, 1973).

A complementary approach to overcome these problems is the use of X-ray microscopy. The higher penetration power of X-rays combined with recent advances in X-ray diffractive optics have led to the implementation of full-field transmission X-ray microscopes with spatial resolution in the 20 nm range (Chao et al., 2005; Schneider et al., 2003). This resolving power together with the use of soft X-rays (with wavelengths in the range of the water window, i.e., 2.3–4.4 nm), provides the possibility to obtain high contrast images from several microns thick unstained biological samples, thus opening a most interesting alternative for supramolecular resolution analysis of biological material. As in the case of cryo-ET, the combination of X-ray imaging with the preservation of the samples at cryogenic temperatures is required to retrieve structural and chemical information close to physiological conditions, as well as to minimize the effect of radiation damage on biological samples (Schneider, 1998). Furthermore, the small numerical aperture and, therefore, relatively large depth of focus of zone plate objectives allows collecting tomographic tilt series to render three-dimensional volumes of thick samples such as

\* Corresponding author. Address: Centro Nacional de Biotecnología, Consejo Superior de Investigaciones Científicas (CSIC), Campus Universidad Autónoma, Department of Structure of Macromolecules, Cantoblanco, Madrid 28049, Spain. Fax: +34 915854506.

E-mail address: [jlcarra@cnb.csic.es](mailto:jlcarra@cnb.csic.es) (J.L. Carrascosa).

algae (Weiss et al., 2000) and other whole cells (Gu et al., 2007; Larabell and Le Gros, 2004; Parkinson et al., 2008; Schneider et al., 2002).

The present potential of cryo-X-ray tomography (cryo-XT) for three-dimensional imaging of fully hydrated biological samples is under expansion. Technical challenges involved in different aspects of the technique are under extensive improvement, as is the use of high resolution X-ray objectives (zone plates), while solutions to other problems such as accurate cryo-sample stages and holders for full-field microscopy were developed. An intensive qualitative work has been carried out to explore the possibilities of XT with whole cells (Gu et al., 2007; Larabell and Le Gros, 2004; Le Gros et al., 2005; Schneider et al., 2002; Thieme et al., 2003; Weiss et al., 2000) yielding morphological descriptions of cell organelles and segmentation of cellular contents based on differential absorption properties (Weiss et al., 2000; Parkinson et al., 2008). Nevertheless, quantitative tests of the cryo-XT resolution capability and performance in biology need to be examined. One of the underlying questions along with these developments is the definition of the resolution actually attained with biological materials, i.e., which are the biological structures resolvable using this imaging technique. In an attempt to get an insight into this issue, we have studied vaccinia virus as test sample. This member of the Poxviridae family is the largest and most complex animal virus (Moss, 2007), with a brick shape, measuring  $360 \times 270 \times 250 \text{ nm}^3$  (Cyrklaff et al., 2005; Moss, 2007). There are two infection forms of the virus, called mature virus (MV) and enveloped virus (EV), which differ in the number of membranes and exert different roles in the virus life cycle (Roberts and Smith, 2008). The structure of the most abundant MV virus has been solved using different microscopy techniques, including cryo-ET (Cyrklaff et al., 2005, 2007; Dubochet et al., 1994; Griffiths et al., 2001a,b). It comprises an outer single membrane that encloses an inner core, constituting a particle containing about 100 different protein species. The core itself shows an external membrane modified with a layer of protein, and an inner cavity where dense nucleoprotein coils are arranged in an irregular fashion (Cyrklaff et al., 2005). Thus, the different structural components of the virus, including membranes and cavities of different density are used to demonstrate the capabilities of cryo-XT.

## 2. Materials and methods

### 2.1. Viral preparation

The attenuated vaccinia virus M65 derived from the WR strain during virus persistence (Dallo et al., 1989; Paez et al., 1985, 1987) was grown in BSC40 cells and purified by banding on sucrose gradients as described in Esteban (1984).

### 2.2. Sample preparation for electron microscopy

Samples of purified vaccinia virus M65 in PBS (phosphate buffered saline) were sonicated twice for 5 s in an ultrasonic bath (Branson 250) at 4 °C to disperse virus aggregates. Then the viral sample was submitted to a mild fixation with 0.1% glutaraldehyde for 15 min at 4 °C, followed by an incubation at room temperature for 5 min with  $\text{NH}_4\text{Cl}$  10 mM to quench the unreacted aldehyde groups. To check the homogeneity and purity of the prepared sample, an aliquot was negatively stained with 2% uranyl acetate for visualization on a JEOL JEM-1011 electron microscope operating at 100 kV. The preparation for the samples used for the resolution calculation of the cryo-ET is described in Cyrklaff et al. (2005).

### 2.3. Sample preparation for cryo X-ray microscopy

Samples of purified vaccinia virus M65 (4  $\mu\text{l}$ ) were loaded on glow discharged bare copper grids for 1 min at room temperature. A volume of 2  $\mu\text{l}$  was removed from the grid before frontal blotting (1 s) using Whatman® 1 paper. Fast freezing was performed by plunge-freezing on a Leica EM-CPC using nitrogen-cooled liquid ethane (−178 °C). The vitrified grids were maintained at liquid nitrogen temperature in a container for storage before data collection. Note that no staining was used for cryo-XT.

### 2.4. Cryo-X-ray tomography

The full-field transmission X-ray microscope at the undulator beamline U41 at the BESSY II electron storage ring (Berlin, Germany) was used (Schneider et al., 2007) to record tilt series of  $\pm 65^\circ$  at 2.43 nm wavelength (photon energy  $E = 510 \text{ eV}$ ). A complete tomographic data set using a constant  $1^\circ$  tilt increment yielded 131 projections in 35 min. The condenser is a single-bounce ellipsoidal glass capillary manufactured by XRADIA (Zeng et al., 2008) with a working distance of about 5 mm and a focal spot size of about 1  $\mu\text{m}$  FWHM (Guttmann et al., 2008). Therefore, the condenser is helically scanned to generate a homogeneously illuminated object field (field of view ranging from 7 to 25  $\mu\text{m}$  for this study). The sample stage is constituted by an FEI compustage modified for X-ray synchrotron beam geometry and a Gatan model 630 cryo-holder. The advantage of this sample stage is that the specimen can be adjusted to the eucentric axis of the stage. Therefore, no realignment or refocusing is necessary over the whole tilt range due the high stability of the design, allowing us to use an exposure time of 2 s per projection without image drift artifacts. The image is formed by Fresnel objective zone plates manufactured at the Helmholtz Zentrum Berlin. Two different zone plate objectives were used: one high resolution objective with 900 zones, focal length of 0.925 mm (at  $E = 510 \text{ eV}$ ) and outermost zone width of  $\text{dr}_N = 25 \text{ nm}$ , and another medium resolution objective for larger depth of field with 560 zones, focal length of 1.5 mm (at  $E = 510 \text{ eV}$ ) and outermost zone width of  $\text{dr}_N = 40 \text{ nm}$ . In general, the resolution depends on the numerical apertures of both the condenser used for the object illumination and the objective (Born and Wolf, 1980). As the BESSY full-field transmission X-ray microscope uses partially coherent light, smallest lines and spaces of 17 nm for the 25 nm zone plate are detectable with the described optical setup. The monochromatized photon flux impinging on the sample is on the order of  $10^9 \text{ photons}/(\mu\text{m}^2 \text{ s})$ . The enlarged projections formed by the zone plate objective were recorded by a Peltier-cooled, back-thinned, direct-illuminated  $1340 \times 1300$  pixel soft X-ray CCD camera (Roper Scientific PI-SX 1300) with a pixel size of 20  $\mu\text{m}$ . For cryo-XT a magnification of 2305-fold corresponding to an image pixel size of 8.68 nm at 510 eV photon energy was used.

### 2.5. Image processing

The tilt series were processed in a Fujitsu-Siemens Celius V810 bi-opteron with 16 GB of RAM running Linux. The raw images were converted to MRC stacks and pre-processed and aligned using the IMOD software package (Kremer et al., 1996) without fiducial markers as a first step. The stacks were cropped to avoid CCD border artifacts and realigned using the viral particles as fiducials with an IMOD calculated residual errors mean value of around 4 pixels. The final aligned tilt series were normalized and reconstructed using the weighted-backprojection algorithms implemented in the IVE/Priism software package (Chen et al., 1996; Hans et al., 1992).

## 2.6. Resolution assessment

The resolution of the cryo-XT datasets was assessed according to the  $FSC_{e/o}$  criterion (Cardone et al., 2005) using programs based on the Bsoft software package (Heymann and Belnap, 2007). In order to maximize the signal and to avoid an underestimation of the quality of the dataset, the  $FSC_{e/o}$  was computed over a set of selected sub-tomograms containing vaccinia virions. The final resolution was determined at a threshold of 0.25 of the  $FSC_{e/o}$  curve (Cardone et al., 2005; Rosenthal et al., 2003). For comparison, sub-tomograms extracted from cryo-ET datasets (Cyrklaff et al., 2005) were processed using the same procedure to estimate the resolution.

## 3. Results and discussion

Vaccinia virus M65 (Paez et al., 1985), derived from the WR strain during virus persistence in culture cells, is a highly attenuated virus (Dallo et al., 1989; Paez et al., 1987). Virus produced in adapted monkey kidney BSC40 cell cultures were purified to render a population of around  $1.3 \times 10^{10}$  pfu/ml. These purified virus preparations representing the MV form showed a relatively homogeneous aspect, where viral particles were easily found (Fig. 1). The general structure of the virus was essentially as described in previous publications (reviewed in Condit et al., 2006; Moss, 2007), depicting a rectangular profile with surface corrugations of the external membrane well contrasted by the staining reagent (Fig. 1, inset). Dimensions of the virus ranged from 270 to 350 nm, depending on the viewing angle.

Different aliquots of the virus preparation were applied to microscope grids covered either with carbon, plastic and carbon, or without any sustaining surface, before plunge-freezing in liquid ethane. The layer thickness of the sample was adjusted between 3

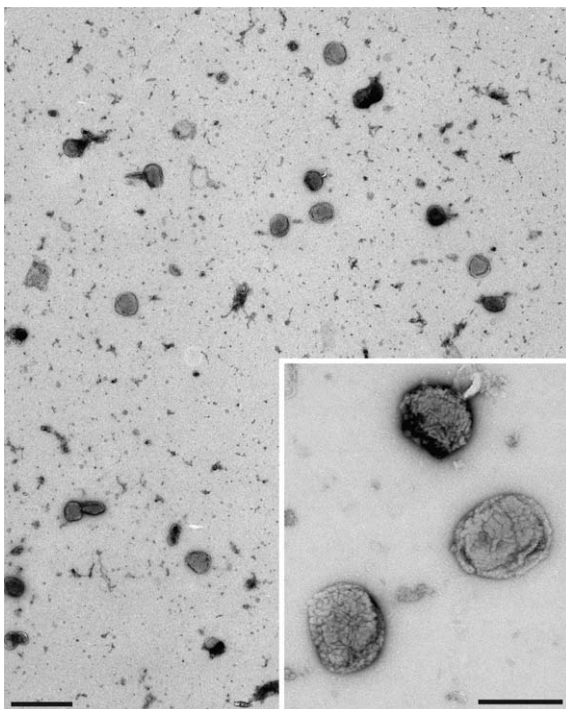


**Fig. 1.** Electron micrographs of negatively stained particles from vaccinia virus M65 derived from the WR strain. Low magnification field of the viral preparation. Scale bar represents 1  $\mu$ m. The inset shows the viral particles at a higher magnification. Scale bar represents 300 nm.

and more than 12  $\mu$ m to mimic the conditions characteristic for the window of applications suitable for X-ray imaging and tomography which are not accessible for cryo-ET. The samples were transferred into the X-ray microscope using a modified transmission electron microscopy cryo-holder at liquid nitrogen temperature. The temperature during image acquisition was maintained at  $-170$  °C. Projection images were taken at 510 eV using the BESSY full-field transmission X-ray microscope (Schneider et al., 2006) equipped with a zone plate objective of 25 nm outermost zone width. Due to the flat nature of the sample holder, X-ray imaging was straightforward after focus adjustment for each area. Areas suitable for tomography were selected on the basis of their average density and high contrast. In these areas, viruses were readily found as rounded objects with a contrast well above the vitreous ice embedding layer. The best areas were found in samples prepared on bare grids without any sustaining substrate. Tilting of the sample up to  $65^\circ$  allowed obtaining well contrasted images where the viruses were still clearly recognizable. Tomographic datasets were obtained using a high precision goniometer that rotated the sample between  $\pm 65^\circ$  at  $1^\circ$  intervals. For each tomographic series 131 images with an exposure time of 2–2.6 s per image were collected. Before and after the acquisition of the tilt series, two images at  $0^\circ$  tilt were recorded. No radiation damage, neither in the virus aspect nor in the ice structure, was apparent from the comparison of the two images.

The projection images from each tomographic series were aligned using the viral particles themselves as fiducial markers. The aligned tilt series were reconstructed by weighted-backprojection algorithm. The three-dimensional reconstructed volume revealed the viral particles even without any segmentation procedure. An example is shown in Fig. 2, where a fairly uniform distribution of viral particles is found in the front view of the volume (Fig. 2a). Side sections of the reconstruction revealed the thickness of the reconstructed ice volume (ranging from 3.5 to 5  $\mu$ m). Interestingly, although several viral particles were found well inside the embedding ice, most viruses were found near the two surfaces of the ice (Fig. 2b). The preferential localization of protein complexes near the surface of aqueous solutions has been previously reported for other tomographic reconstructions from cryo-electron microscopy.

Due to the excellent natural contrast between the unstained virus particles and the surrounding ice layer of the reconstructed volume, it was possible to see structural features within the X-ray reconstructed virions (Fig. 3a). A gallery of representative planes taken from a set of sub-tomograms corresponding to different viral particles (Fig. 3b) shows the consistent presence of an external envelope in the viral particles. In addition, the interior of the particles shows an inner region comprising a lighter core surrounded by a denser envelope. Sometimes the inner core was centered, while in other particles it was located besides the external envelope.

The resolution of the different datasets was assessed according to the  $FSC_{e/o}$  criterion (Cardone et al., 2005). To estimate the highest resolution attainable under the present experimental conditions, tomograms were obtained using the  $dr_N = 25$  nm zone plate (see Section 2). The tilt series were split into two halves corresponding to the even and odd projection images, respectively. Two independent tomograms were computed from the tilt series halves. As the whole tomograms contained significant background, the  $FSC_{e/o}$  criterion computed from them substantially underestimated the effective resolution (Cardone et al., 2005). Therefore, the  $FSC_{e/o}$  criterion was then computed from a set of representative sub-tomograms in order to improve the amount of signal against the background and thus obtain a more accurate estimate of the quality of the dataset. Twenty sub-tomograms containing vaccinia virions were then extracted from each of the two independent

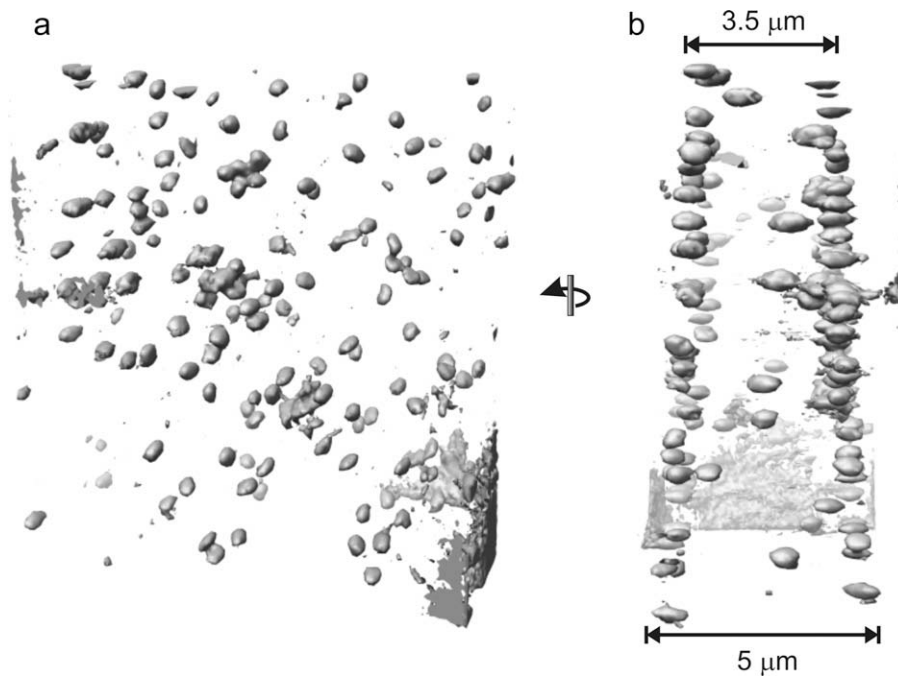


**Fig. 2.** Three-dimensional rendering from the X-ray tomographic reconstructed volume using a 40 nm zone plate. (a) Front view. (b) Side view of the reconstructed volume where the thickness of the sample is indicated.

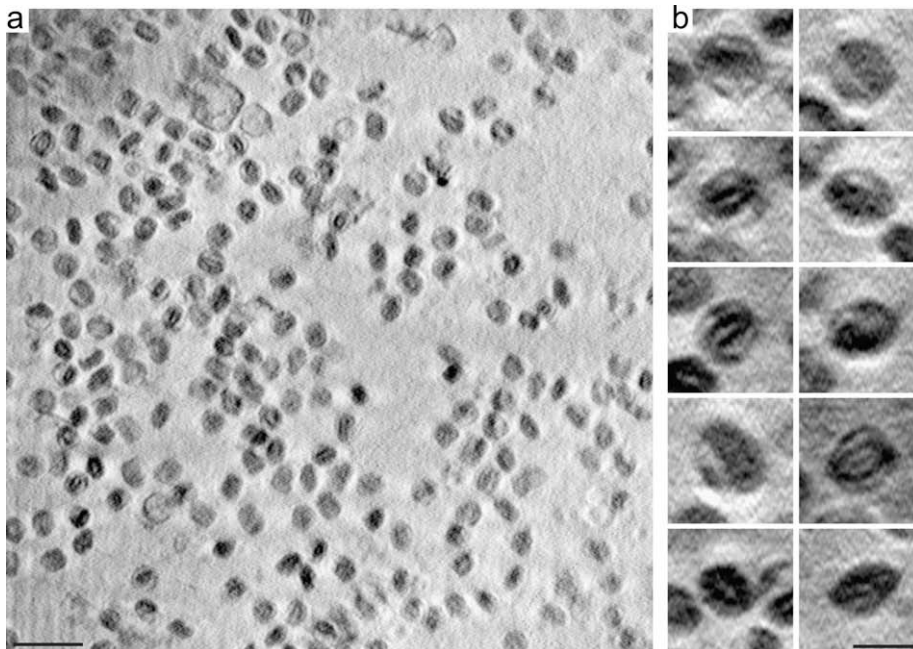


**Fig. 3.** X-ray tomographic reconstruction of the vaccinia virus particles acquired with a 25 nm zone plate. (a) Oblique slice extracted from a tomogram. Scale bar represents 1  $\mu\text{m}$ . (b) Central slices of subvolumes extracted from the tomogram, each containing a different viral particle. Internal features within each virion are visible. Scale bar represents 300 nm.

tomograms. The  $FSC_{e/o}$  curve was computed from the whole set of 20 sub-tomograms, obtaining a final resolution of 25.7 nm half-pitch (Fig. 4). A similar calculation using the datasets obtained from cryo-electron tomograms (Cyrklaff et al., 2005) revealed a nominal resolution of 6.7 nm half-pitch. Thus, the equivalent resolution ratio between X-ray and electron tomograms is about 3.8 for the same type of samples prepared under the same conditions.

The structural features found for the X-ray reconstructed vaccinia virions are fully consistent with the structure of the vaccinia virus known from electron microscopy using either thin sections (Griffiths et al., 2001a), cryo-electron microscopy projections (Cyrklaff et al., 2007; Dubochet et al., 1994) or tomograms (Cyrklaff et al., 2005). Fig. 5a shows two representative planes from cryo-X-ray tomographic virus reconstructions where the inner core is placed off-centre inside the outer envelope. These images correlate

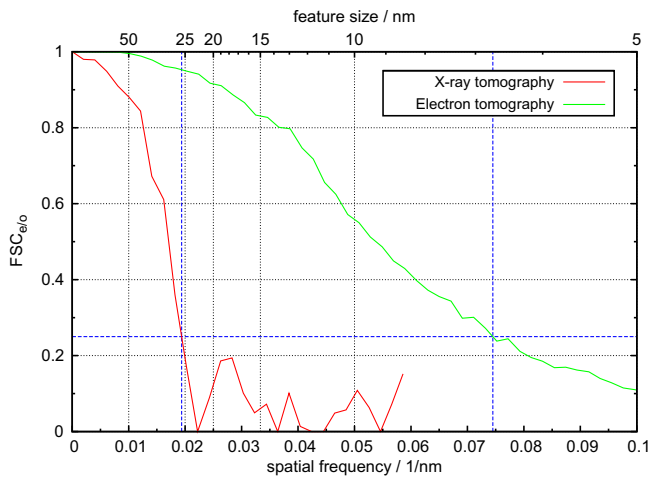


**Fig. 4.** Resolution comparison between cryo-X-ray and cryo-electron tomography resolution estimated with the  $FSC_{e/o}$  curves computed from sub-tomograms using a threshold of 0.25. According to the  $FSC_{e/o}$  curve, the final resolution of the X-ray dataset acquired with a zone plate of 25 nm was found to be 25.7 nm half-pitch and 0.0194 1/nm spatial frequency. The  $FSC_{e/o}$  curve from the set of cryo-ET was computed from the data in Cyrklaff et al. (2005), and it was found to be 6.7 nm half-pitch and 0.0746 1/nm spatial frequency.

well with the images from cryo-electron tomographic reconstructed vaccinia virus (Cyrklaff et al., 2005), where the different compartments are seen, albeit at higher magnification (Fig. 5b). The viral outer membrane encloses an inner core containing the nucleoprotein of the virus. The inner region of the core shows a lighter density, probably consistent with the irregular distribution of the nucleoprotein within the core (Cyrklaff et al., 2005). In the X-ray tomograms, just besides the outer viral envelope, the virus presents one conspicuous structural feature, the so-called lateral body (similar to the observed from the datasets from Cyrklaff et al., 2005, Fig. 5a). Another characteristic view of the X-ray

reconstructed virions is the one where the inner core is placed in the centre of the virion (Fig. 5c), a view that might be readily correlated with the typical dumbbell shaped core seen in electron tomographic reconstructions (Fig. 5d, obtained from the datasets in Cyrklaff et al., 2005).

Our results show that, although the resolution limit imposed by the outermost zone width (25 nm) of the X-ray objective is well above the size of the putative virus membranes, even when they are modified by protein insertion and attachment (6–18 nm), they were easily identified due to their strong differential absorption contrast against the surrounding ice layer. Furthermore, inner details of the virus are distinguishable such as the core shape and its internal distribution of material. Therefore, cryo-XT reveals the three-dimensional structure of complex biological structures showing envelopes and compartments well beyond the nominal X-ray optical resolution of the microscope. Note that this observation is not in contradiction to microscopy principles as these features smaller than the resolution limit determined by the numerical aperture of the X-ray objective, together with the numerical aperture of the condenser, can be visualized in the reconstructions but their size cannot be measured.

In conclusion, we propose that cryo-X-ray tomography at 510 eV photon energy is able to retrieve structural information from thick samples containing biological material with such a high intrinsic contrast so as to detect membrane-bound compartments, or envelopes, in a relatively complex macromolecular aggregate like vaccinia virus. The use of a well-defined biological specimen has allowed comparing the performance of two tomographic approaches (X-rays and electrons) using single-particle analysis techniques to evaluate the respective attained resolutions (X-rays/e<sup>-</sup> ratio ~3.8). Although the present resolution limit imposed by the X-ray objective during these experiments does not allow obtaining precise measurements of the features detected so far, X-ray microscopy opens an interesting possibility for investigating thick samples at sub-cellular level and, in particular, the challenging study of the process of the viral live cycle within infected cells.

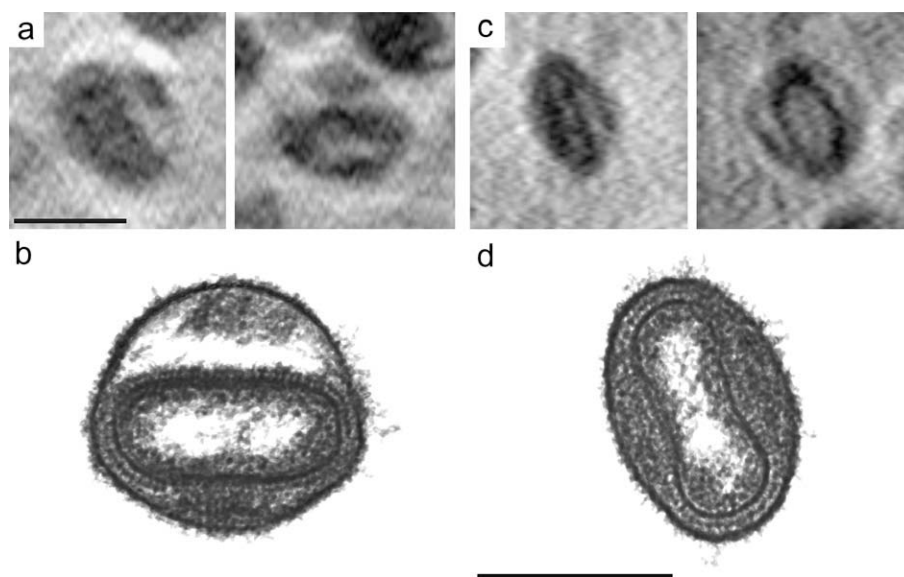


**Fig. 5.** Comparison between the structural features of vaccinia virus revealed by cryo-X-ray tomography and cryo-electron tomography. (a) Viral particles with inner core placed off-centre inside the outer envelope from X-ray tomography: central planes from sub-tomograms extracted from X-ray tomography. (b) Viral particles with inner core placed off-centre inside the outer envelope from cryo-electron tomography (the same dataset from Fig. 3 in Cyrklaff et al. (2005)). (c) Viral particles with inner core centred inside the outer envelope from X-ray tomography. (d) Viral particles with inner core centred inside the outer envelope from cryo-electron tomography (the same dataset from Fig. 2 in Cyrklaff et al. (2005)). The scale bars represent 300 nm.

## Acknowledgments

This work was supported by Grants BFU2008-2328/BMC (to J.L.C.), LSHG-CT-2004-502828 (to J.L.C.), CT-2006-037536 and Foundation Botín (to M.E.), BESSY-EC-IA-SFS (EU support for the experiments at BESSY), by the German Federal Ministry of Education and Research (BMBF) under contract number 05KS4BY1/7, by the Human Frontier Science Program (HFSP) Research Grant Ref. RGP0053/2005-C and by the EU in the 6th framework program under contract number RII3-CT-2004-506008.

## References

- Born, M., Wolf, E., 1980. Chapter X: Interference and Diffraction with Partially Coherent Light, Principles of Optics. Pergamon Press, Oxford.
- Cardone, G., Grunewald, K., Steven, A.C., 2005. A resolution criterion for electron tomography based on cross-validation. *J. Struct. Biol.* 151, 117–129.
- Condit, R.C., Moussatche, N., Traktman, P., 2006. In a nutshell: structure and assembly of the vaccinia virion. *Adv. Virus Res.* 66, 31–124.
- Cyrklaff, M., Risco, C., Fernandez, J.J., Jimenez, M.V., Esteban, M., Baumeister, W., Carrascosa, J.L., 2005. Cryo-electron tomography of vaccinia virus. *Proc. Natl. Acad. Sci. USA* 102, 2772–2777.
- Cyrklaff, M., Linaroudis, A., Boicu, M., Chlanda, P., Baumeister, W., Griffiths, G., Krijnse-Locker, J., 2007. Whole cell cryo-electron tomography reveals distinct disassembly intermediates of vaccinia virus. *PLoS ONE* 2, e420.
- Chao, W., Harteneck, B.D., Liddle, J.A., Anderson, E.H., Attwood, D.T., 2005. Soft X-ray microscopy at a spatial resolution better than 15 nm. *Nature* 435, 1210–1213.
- Chen, H., Hughes, D.D., Chan, T.A., Sedat, J.W., Agard, D.A., 1996. IVE (Image Visualization Environment): a software platform for all three-dimensional microscopy applications. *J. Struct. Biol.* 116, 56–60.
- Dallo, S., Maa, J.S., Rodriguez, J.R., Rodriguez, D., Esteban, M., 1989. Humoral immune response elicited by highly attenuated variants of vaccinia virus and by an attenuated recombinant expressing HIV-1 envelope protein. *Virology* 173, 323–329.
- Dubochet, J., Adrian, M., Richter, K., Garces, J., Wittek, R., 1994. Structure of intracellular mature vaccinia virus observed by cryoelectron microscopy. *J. Virol.* 68, 1935–1941.
- Esteban, M., 1984. Defective vaccinia virus particles in interferon-treated infected cells. *Virology* 133, 220–227.
- Frank, J., 2006. Electron Tomography, Methods for Three-dimensional Visualization of Structures in the Cell, second ed. Springer, New York.
- Fung, J.C., Liu, W., de Ruijter, W.J., Chen, H., Abbey, C.K., Sedat, J.W., Agard, D.A., 1996. Toward fully automated high-resolution electron tomography. *J. Struct. Biol.* 116, 181–189.
- Griffiths, G., Roos, N., Schleich, S., Locker, J.K., 2001a. Structure and assembly of intracellular mature vaccinia virus: thin-section analyses. *J. Virol.* 75, 11056–110570.
- Griffiths, G., Wepf, R., Wendt, T., Locker, J.K., Cyrklaff, M., Roos, N., 2001b. Structure and assembly of intracellular mature vaccinia virus: isolated-particle analysis. *J. Virol.* 75, 11034–11055.
- Grunewald, K., Cyrklaff, M., 2006. Structure of complex viruses and virus-infected cells by electron cryo tomography. *Curr. Opin. Microbiol.* 9, 437–442.
- Gu, W., Etkin, L.D., Le Gros, M.A., Larabell, C.A., 2007. X-ray tomography of *Schizosaccharomyces pombe*. *Differentiation* 75, 529–535.
- Guttman, P., Zheng, X., Feser, M., Heim, S., Yun, W., Schneider, G., 2008. Ellipsoidal capillary as condenser for the BESSY full-field X-ray microscope. In: IOP Ninth International Conference on X-ray Microscopy, Zürich, Switzerland.
- Hans, C., Warren, K.C., John, W.S., Agard, D.A., 1992. In: Raj, S.A. et al. (Eds.), PRIISM: An Integrated System for Display and Analysis of 3D Microscope Images, vol. 1660. SPIE, pp. 784–790.
- Heymann, J.B., Belnap, D.M., 2007. Bsoft: image processing and molecular modeling for electron microscopy. *J. Struct. Biol.* 157, 3–18.
- Kremer, J.R., Mastrorade, D.N., McIntosh, J.R., 1996. Computer visualization of three-dimensional image data using IMOD. *J. Struct. Biol.* 116, 71–76.
- Larabell, C.A., Le Gros, M.A., 2004. X-ray tomography generates 3D reconstructions of the yeast, *Saccharomyces cerevisiae*, at 60-nm resolution. *Mol. Biol. Cell* 15, 957–962.
- Le Gros, M.A., McDermott, G., Larabell, C.A., 2005. X-ray tomography of whole cells. *Curr. Opin. Struct. Biol.* 15, 593–600.
- Lucic, V., Forster, F., Baumeister, W., 2005. Structural studies by electron tomography: from cells to molecules. *Annu. Rev. Biochem.* 74, 833–865.
- Moss, B., 2007. Poxviridae: the viruses and their replication. In: Knipe, D.N., Howley, P.M. (Eds.), *Fields Virology*. Lippincott Williams & Wilkins, a Wolters Kluwer Business, Philadelphia, pp. 2905–2975.
- Paez, E., Dallo, S., Esteban, M., 1985. Generation of a dominant 8-MDa deletion at the left terminus of vaccinia virus DNA. *Proc. Natl. Acad. Sci. USA* 82, 3365–3369.
- Paez, E., Dallo, S., Esteban, M., 1987. Virus attenuation and identification of structural proteins of vaccinia virus that are selectively modified during virus persistence. *J. Virol.* 61, 2642–2647.
- Parkinson, D.Y., McDermott, G., Etkin, L.D., Le Gros, M.A., Larabell, C.A., 2008. Quantitative 3D imaging of eukaryotic cells using soft X-ray tomography. *J. Struct. Biol.* 162, 380–386.
- Roberts, K.L., Smith, G.L., 2008. Vaccinia virus morphogenesis and dissemination. *Trends Microbiol.* 16, 472–479.
- Rosenthal, P.B., Crowther, R.A., Henderson, R., 2003. An objective criterion for resolution assessment in single-particle electron microscopy (Appendix). *J. Mol. Biol.* 333, 721–745.
- Schneider, G., 1998. Cryo X-ray microscopy with high spatial resolution in amplitude and phase contrast. *Ultramicroscopy* 75, 85–104.
- Schneider, G., Guttman, P., Heim, S., Rehbein, S., Eichert, D., Niemann, B., 2007. X-ray microscopy at BESSY: from nano-tomography to fs-imaging. *Synchrotron Radiation and Instrumentation*, pp. 1241–1294. In: Choi, J.-Y., and Rah, S., (eds.) *Synchrotron Radiation and Instrumentation Proceedings IX International Conference*, Vol. 879. AIP Conf. Proc.
- Schneider, G., Anderson, E., Vogt, S., Knochel, C., Weiss, D., Legros, M., Larabell, C., 2002. Computed tomography of cryogenic cells. *Surf. Rev. Lett.* 9, 177–183.
- Schneider, G., Denbeaux, G., Anderson, E., Pearson, A., Bates, W., Vogt, S., Knochel, C., Meyer, M.A., Zschech, E., 2003. High resolution X-ray tomography with applications in biology and materials science. *J. Phys. IV* 104, 607–613.
- Spence, J.C.H., 2003. *Experimental High-resolution Electron Microscopy*, third ed. Oxford University Press, New York.
- Subramaniam, S., Bartesaghi, A., Liu, J., Bennett, A.E., Sougrat, R., 2007. Electron tomography of viruses. *Curr. Opin. Struct. Biol.* 17, 596–602.
- Thieme, J., Schneider, G., Knochel, C., 2003. X-ray tomography of a microhabitat of bacteria and other soil colloids with sub-100 nm resolution. *Micron* 34, 339–344.
- Tokuyasu, K.T., 1973. A technique for ultracryotomy of cell suspensions and tissues. *J. Cell Biol.* 57, 551–565.
- Weiss, D., Schneider, G., Niemann, B., Guttman, P., Rudolph, D., Schmahl, G., 2000. Computed tomography of cryogenic biological specimens based on X-ray microscopic images. *Ultramicroscopy* 84, 185–197.
- Zeng, X., Duerwer, F., Feser, M., Huang, C., Lyon, A., Tkachuk, A., Yun, W., 2008. Ellipsoidal and parabolic glass capillaries as condensers for X-ray microscopes. *Appl. Opt.* 47, 2376–2381.